Biochimica et Biophysica Acta 1813 (2011) 1220–1229

Contents lists available at ScienceDirect

Biochimica et Biophysica Acta

journal homepage: www.elsevier.com/locate/bbamcr

FTIR spectral signatures of mouse antral oocytes: Molecular markers of oocyte maturation and developmental competence

Diletta Ami [a], Paolo Mereghetti [b,c], Antonino Natalello [d], Silvia Maria Doglia [d,*], Mario Zanoni [e], Carlo Alberto Redi [a,**], Manuela Monti [a]

[a] Fondazione IRCCS Policlinico San Matteo, V.le C. Golgi 19, 27100 Pavia, Italy
[b] BIOMS (Center for Modeling and Simulation in the Biosciences), University of Heidelberg, Im Neuenheimer Feld 36, 69120 Heidelberg, Germany
[c] Molecular and Cellular Modeling Group, HITS gGmbH, Schloss Wolfsbrunnenweg 35, 69118, Heidelberg, Germany
[d] Dipartimento di Biotecnologie e Bioscienze, Università di Milano-Bicocca, Piazza della Scienza 2, 20126 Milano, Italy
[e] Laboratorio di Biologia dello Sviluppo, Dipartimento di Biologia Animale, Università degli Studi di Pavia, Via A. Ferrata 1, 27100 Pavia, Italy

ARTICLE INFO

Article history:
Received 12 October 2010
Received in revised form 15 February 2011
Accepted 15 March 2011
Available online 22 March 2011

Keywords:
FTIR microspectroscopy
SN oocytes
NSN oocytes
Oocyte maturation
Developmental competence
Polyadenylation

ABSTRACT

Mammalian antral oocytes with a Hoescht-positive DNA ring around the nucleolus (SN) are able to resume meiosis and to fully support the embryonic development, while oocytes with a non-surrounded nucleolus (NSN) cannot. Here, we applied FTIR microspectroscopy to characterize single SN and NSN mouse oocytes in order to try to elucidate some aspects of the mechanisms behind the different chromatin organization that impairs the full development of NSN oocyte-derived embryos. To this aim, oocytes were measured at three different stages of their maturation: just after isolation and classification as SN and NSN oocytes (time 0); after 10 h of in vitro maturation, i.e. at the completion of the metaphase I (time 1); and after 20 h of in vitro maturation, i.e. at the completion of the metaphase II (time 2). Significant spectral differences in the lipid (3050–2800 cm^{-1}) and protein (1700–1600 cm^{-1}) absorption regions were found between the two types of oocytes and among the different stages of maturation within the same oocyte type. Moreover, dramatic changes in nucleic acid content, concerning mainly the extent of transcription and polyadenylation, were detected in particular between 1000 and 800 cm^{-1}. The use of the multivariate principal component–linear discriminant analysis (PCA–LDA) enabled us to identify the maturation stage in which the separation between the two types of oocytes took place, finding as the most discriminating wavenumbers those associated to transcriptional activity and polyadenylation, in agreement with the visual analysis of the spectral data.

1. Introduction

Murine oocytes isolated from the ovarian antral compartment are characterized by two different types of chromatin organization [1,2] as in most mammalian species like the rat [3], the pig [4], the monkey [5] and the human [6]. In the Surrounded Nucleolus (SN) type, chromatin is highly condensed and forms a Hoechst positive ring around the nucleolus, while in the Not Surrounded Nucleolus (NSN) oocytes the chromatin is more dispersed and less condensed around the nucleolus [7]. The important issue of chromatin organization has been studied by several complementary techniques, such as confocal fluorescence microscopy [8] and transmission electron microscopy [6,9]. For oocytes, chromatin organization and regulation of transcription are strictly related to each other, as it is well known that heterochromatic chromatin is associated with low level of transcription. For this reason, SN oocytes are considered transcriptionally inactive while the NSN types are transcriptionally active [1,2,6]. Another important difference between SN and NSN antral oocytes concerns their ability to resume meiosis and complete, after fertilization, the embryonic development: only the SN type is able to develop till the blastocyst stage while the NSN type arrests its development at the two cell stage.

It is still unknown how the well orchestrated functional ovary originates oocytes with different destiny and which are the molecular events accounting for the two different chromatin organizations and thus two different prospective zygotic developments.

It has been suggested that the NSN-derived zygotic epigenome shows reduced levels of expression of some important genes involved

Abbreviations: A, Adenine; CPE, cytoplasmic polyadenylation element; CpG, Cytosine-phosphate-Guanine; FTIR, Fourier Transform InfraRed; GV, Germinal vesicle; GVBD, Germinal vesicle break down; MCT, Mercury cadmium telluride; MI, Metaphase I; MII, Metaphase II; mRNA, messenger RNA; NSN, not surrounded nucleolus; PCA–LDA, Principal component analysis–linear discriminant analysis; polyA, polyAdenyne; SN, Surrounded nucleolus; U, Uracil

* Correspondence to: S.M. Doglia, Dipartimento di Biotecnologie e Bioscienze, Università di Milano-Bicocca, Piazza della Scienza 2, 20126 Milano, Italia. Tel.: +39 02 64483459; fax: +39 02 64483565.
** Correspondence to: Prof. Carlo Alberto Redi, Dipartimento di Biologia Animale, Università degli Studi di Pavia, Via Ferrata 1, 27100 Pavia, Italy. Tel.: +39 0382 986306; fax: +39 0382 986270.
E-mail addresses: silviamaria.doglia@unimib.it (S.M. Doglia), carloalberto.redi@unipv.it (C.A. Redi).

0167-4889/$ – see front matter © 2011 Elsevier B.V. All rights reserved.
doi:10.1016/j.bbamcr.2011.03.009

in cell differentiation, transcription and fatty acid oxidation [8,10]. For instance, previous experiments performed on single antral oocytes showed that the well known transcription factor Oct4 is detected with very low levels of expression in the NSN compared to the SN type: this might explain the greater developmental capacity of the SN oocytes and its correlation with the totipotent characteristic of the future zygote [10,11].

To get new insights on the SN and NSN oocyte molecular composition and organization, we used Fourier transformed infrared (FTIR) microspectroscopy, a powerful tool that allows to obtain information on complex biological systems in a non-invasive way. This technique has been widely employed in recent years to study intact cells [12–15], tissues [16–18], whole organisms [19] and to monitor *in situ* biological processes as, for instance, protein aggregation [20,21] and stem cell differentiation [13,22]. In particular, FTIR microspectroscopy allowed to identify spectral markers of putative stem cell populations in different systems, such as bovine and human cornea [23,24] and intestinal crypts [25]. Moreover, FTIR microspectroscopy has been recently employed to characterize pluripotent human embryonic and multipotent human mesenchymal stem cells, highlighting the role of lipids in the discrimination between the two different cell types [26].

In the present paper, we applied FTIR microspectroscopy to study single SN and NSN mouse oocytes at different maturation stages: antral germinal vesicle (GV), metaphase I (MI, collected from isolated SN and NSN oocytes matured for 10 h *in vitro*) and metaphase II (MII, collected from isolated SN and NSN oocytes matured for 20 h *in vitro*). Mammalian oocytes are arrested in different stages of meiotic division: during the first meiotic prophase the immature oocytes are in the GV stage characterized by a de-condensed transcriptionally active chromatin [27]. Meiotic maturation is characterized by germinal vesicle breakdown (GVBD) followed by MI and MII, which is in an arrested stage till the fertilization occurs. Taking into account the intrinsic heterogeneity of the biological samples and the complexity of their infrared absorption, we used a multivariate statistical analysis to validate and better comprehend the spectroscopic data. In particular, the use of the combined principal component analysis–linear discriminant analysis (PCA–LDA) [28,29] allowed us to recognize and pull out the most significant spectral bands that contribute to the largest spectral variance.

2. Materials and methods

2.1. Oocyte isolation and culture

For FTIR characterization, oocytes were collected at different times of their maturation - GV, MI and MII stages - to get a dynamic view of protein and nucleic acid contents. Female mice B6D2F1 (F1 CD^{-1}), purchased from Charles River (Como, Italy), were maintained at the Department Animal Facility of the University of Pavia. Six 12-week-old females were used in this study. Animals were maintained under controlled room conditions (22 °C, with 60% air moisture and 14L:10D photoperiod and fed *ad libitum*) and investigations were conducted in accordance with the guiding principles of European (n. 86/609/CEE) and Italian (n. 116/92, 8/94) laws protecting animals used for scientific research.

GV oocytes were isolated from the antral compartment and classified into SN and NSN types according to the presence or absence of a ring of Hoechst-positive chromatin surrounding the nucleolus (see Fig. 1), as already described [7], and directly used for FTIR analysis. SN and NSN oocytes were matured *in vitro* (α-mem media) [30] to collect MI (after 10 h) and MII (after 20 h) respectively.

For FTIR analysis GV, MI and MII oocytes were washed several times in a 0.9% NaCl aqueous solution to prevent medium contamination. For each cell type, single oocytes were deposited onto a BaF_2 window and dried at room temperature for about 30 min [13]. To verify that this span of time was enough to dry the samples in a reproducible way, we measured the FTIR absorption spectra of oocytes at different times of dehydration, from 30 min up to several hours. Interestingly, comparable results were found for samples dried for 30 min or longer.

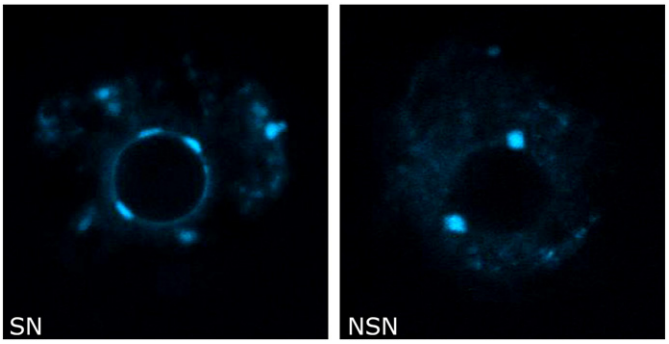

Fig. 1. Nuclei of SN and NSN antral oocytes stained with the fluorochrome Hoechst 33342. SN oocytes are characterized by a ring of Hoechst positive heterochromatin surrounding the nucleolus, that is absent in NSN oocytes. Magnification, 100×.

To evaluate spectral reproducibility, at least 10 cells/type were measured in each of the three independent experiments that we carried out.

2.2. FTIR microspectroscopy

FTIR absorption spectra of single mouse oocytes, taken at different maturation stages, were collected from 4000 to 800 cm^{-1} using a UMA 500 infrared microscope equipped with a nitrogen cooled MCT (Mercury Cadmium Telluride) detector (narrow band, 250 μm) and coupled to a FTS-40A spectrometer (both from Bio-Rad, Digilab Division, MA, USA).

Absorption spectra of single intact oocytes, with an excellent signal to noise ratio (noise of 1 mA peak to peak, all over the spectrum), were acquired in transmission mode by setting the microscope diaphragm aperture at about 100 μm × 100 μm, in order to select a whole single oocyte, whose diameter was varying from 80 to 100 μm. The spectra were collected under the following conditions: 2 cm^{-1} spectral resolution, 512 scan coadditions, 20 kHz scan speed and triangular apodization. When necessary, spectra were corrected for residual water vapor absorption.

Spectral analysis was conducted in the spectral range between 4000 and 800 cm^{-1}. To this aim, second derivative spectra were obtained following the Savitsky–Golay method (3rd grade polynomial, 11 smoothing points), after a binomial 13 smoothing points of the measured spectra, using the GRAMS/32 software (Galactic Industries Corporation, USA).

2.3. Multivariate analysis

Statistically significant spectral components were identified from the measured spectra using a combined PCA–LDA analysis [28,29], performed using MatLab R2006a (The Mathworks, USA).

The combined use of PCA and LDA allows to group large multivariate data into different clusters by maximizing the inter-cluster separation and, at same time, ensuring the minimum variability within the cluster [31,32].

The covariance matrix of the raw spectra was diagonalized to obtain the eigenvectors sorted according to the magnitude of the corresponding eigenvalue.

Only the first K eigenvectors, which describe more than the 99.9% of the total variance, were retained. In the studied systems the value of K was between 15 and 17. A set of principal components (PCA scores) was obtained projecting the original data on the subspace defined by the selected eigenvectors. The linear discriminant analysis was then

performed using as input variables the PCA scores and as class variables the different maturation stages.

In order to assess the ability to discriminate into the different maturation stages, the classification accuracy was computed. Given the ensemble of spectra subjected to the classification analysis, the classification accuracy is computed as fraction of spectra correctly classified over the total number of spectra.

In particular, to reduce the bias in the estimation of the accuracy due to possible outliers, a leave-one-out cross validation was performed. The selection of the most relevant wavenumbers was performed considering the weighted sum of the PCA–LDA [33] defined as $\overline{wl} = \frac{1}{N}\sum_{i=1}^{N} L\,diag\,(C)$, where N is the total number of discriminant functions, L is the PCA–LDA weight matrix obtained using a linear regression of the PCA–LDA score and the original variables and C is the total covariance matrix [28]. The obtained averaged weights are then rescaled in the range of 0–1.

Two dimensional PCA–LDA score plot can be used to visualize clusters. To better visualize the separation among clusters, ellipses (2D plot) were drawn centered on cluster mean, where the semi-axes correspond to two standard deviations of the data. In the 3D score plots, the spread of the data within each cluster is represented by the ellipsoid, whose semi-axes are given by two standard deviations of the data along each direction.

In the figures of the paper, as representative of each oocyte class, we reported the FTIR spectra taken from the centroid of each cluster.

3. Results and discussion

In this paper we measured the FTIR absorption spectra of single SN and NSN mouse oocytes at three different times: just after isolation and classification of antral oocytes (time 0), after *in vitro* maturation of both SN and NSN at the completion of the MI phase, i.e. 10 h after isolation (time 1) and after *in vitro* maturation of both SN and NSN at the completion of the MII phase, i.e. 20 h after isolation (time 2). The resulting spectra, reported in Fig. 2, are very complex and give information on the total biomolecule content of the cell. Indeed, within a single measurement it is possible to obtain simultaneously the infrared response of lipids, proteins and nucleic acids, whose absorptions cover a wide range of frequencies in the mid infrared [34–36]. To resolve the different bands of the spectra we used the second derivative analysis of the data, as described in Materials and methods. By doing this, the different band components in the absorption spectrum correspond to the minima in the second derivative. This analysis is essential to identify the band peak positions and to assign them to the different biomolecule vibrational modes.

Biological samples are characterized by an intrinsic heterogeneity that can be found likely even within the same cell (e.g. oocytes) population. To overcome this problem, we applied the combined PCA–LDA that enables to identify the most significant spectral components accounting for the differences between the two types of oocytes at different stages of their maturation.

We should report that the use of PCA alone was firstly tested. However, no separation of the spectral data between the two types of oocytes was achieved by this approach (see Supplemental Fig. 1).

3.1. Protein and lipid infrared absorptions during SN and NSN oocyte maturation

3.1.1. SN oocytes

The infrared absorption spectrum in the Amide I region, between 1700 and 1600 cm^{-1}, gives information on the secondary structures of the total protein content of the cells.

The second derivative spectrum of the antral SN (GV) oocytes in the Amide I region (Fig. 3A) is characterized by two main absorption bands at 1658 cm^{-1} and at 1639 cm^{-1} that can be assigned respectively to the

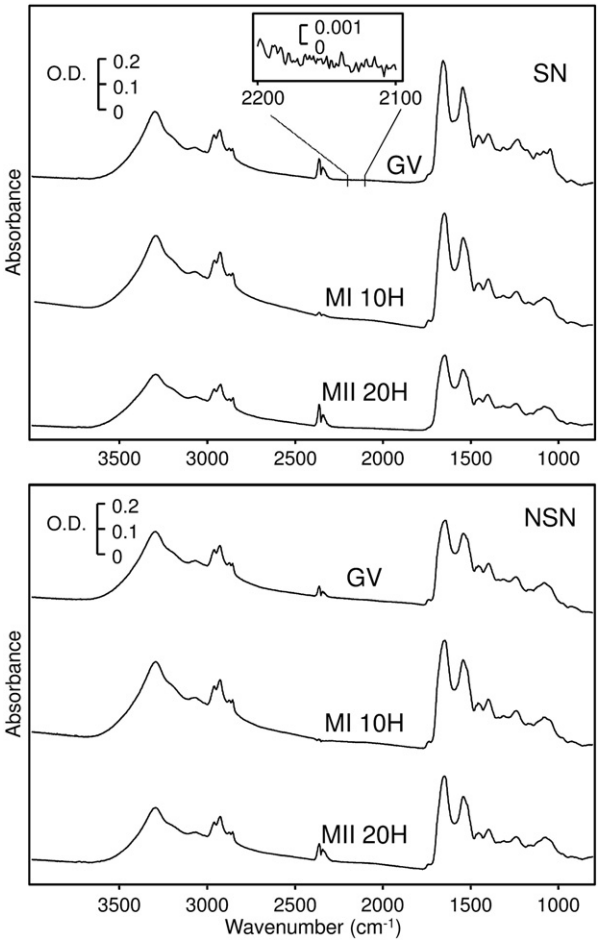

Fig. 2. FTIR absorption spectra of single SN and NSN oocytes. The FTIR absorption spectra of SN and NSN oocytes at each maturation stage (GV, MI, MII) are reported from 4000 to 800 cm^{-1}. Spectra are presented, as measured (without any correction), with their measured absorbance scale and stacked for clarity of presentation. To evaluate the noise level, the 2200–2100 cm^{-1} region is reported in an enlarged scale in the inset.

α-helix and β-sheet secondary structures of the total cell proteins [35,37,38]. In addition, the component at 1690 cm^{-1} can be assigned to β-sheet structures and to protein–protein interactions. These bands were found to vary in intensity and peak position during SN oocyte maturation up to 20 h (time 2, MII oocytes) suggesting that the protein content was changing. Accordingly, several authors [39–41] showed a significant 2-fold change in gene expression during the transition from antral to MII oocytes, suggesting that the acquisition of meiotic competence coincides with a decrease in relative transcript abundance.

In particular, starting from MI, the 1658 cm^{-1} component decreased while that at 1639 cm^{-1} decreased and also downshifted of a few wavenumbers, displaying a shoulder around 1625 cm^{-1}. This latter new component can be assigned to the formation of β-sheet structures and/or to new protein–protein interactions [35,37,38]. Indeed, this result could be explained considering the formation at MI of the meiotic spindle that involves the polymerization of tubulin and the formation of actin microfilaments. In particular, actin is required to mediate peripheral migration of the meiotic spindle, allowing the establishment of polarity and the emission of the first polar body during oocyte maturation [42].

Interestingly, it has been recently highlighted the high potential of the lipid components as important markers of the oocyte developmental competence [14,43]. For this reason, we investigated the lipid absorption between 3050 and 2800 cm^{-1} (data not shown), which gives information mainly on the acyl chain vibrations [34]. The spectrum in this region is dominated by the CH_2 bands occurring

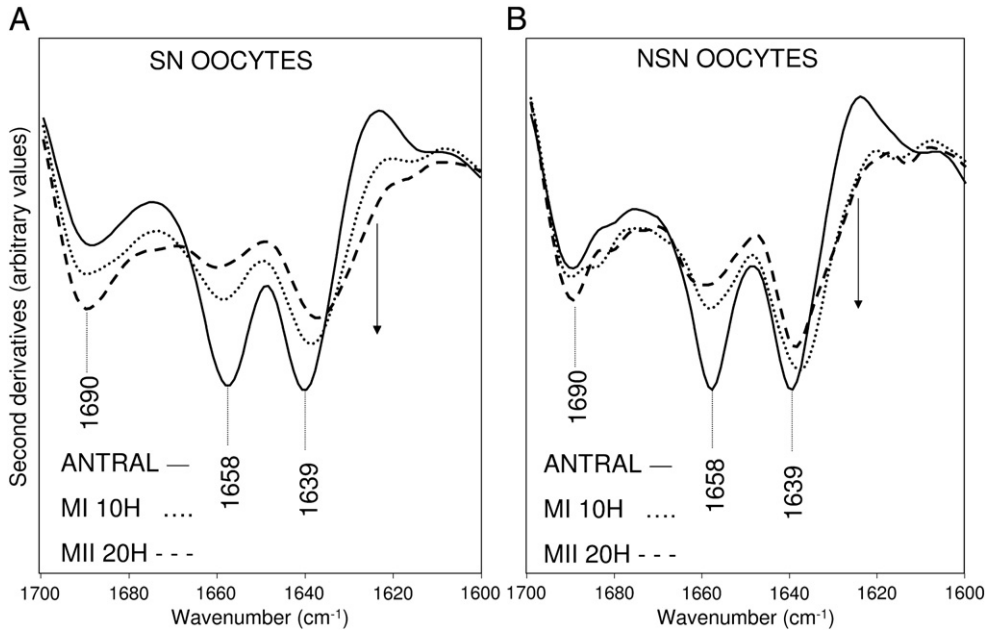

Fig. 3. Second derivative absorption spectra of SN and NSN oocytes in the protein absorption region. The second derivatives of the FTIR absorption spectra of SN (A) and NSN (B) single oocytes, measured at the antral (continuous line), MI (dotted line) and MII (dashed line) stages, are reported in the Amide I region. The main absorption components can be assigned to beta sheet structures (1690 cm^{-1} and 1639 cm^{-1}), alpha helices (1658 cm^{-1}). Arrows point to increasing intensity of the protein–protein interaction component around 1625 cm^{-1}. For comparison, spectra have been normalized at the tyrosine peak around 1516 cm^{-1}.

around 2922 cm^{-1} (antisymmetric stretching) and 2852 cm^{-1} (symmetric stretching) and by the CH_3 bands, around 2960 cm^{-1} (asymmetric stretching) and 2873 cm^{-1} (symmetric stretching). During maturation up MII of SN oocytes, minor but significative changes in the spectral response of the 2922 cm^{-1} CH_2 band were found, due in particular to the increase of a component around 2937 cm^{-1}, likely due to cholesterol and /or phospholipids [44,45], both in the spectrum of antral and MII derived oocytes. Interestingly, cholesterol and phospholipids are known to modulate membrane fluidity, whose role in rapid cell division after fertilization has been recently highlighted by Wood and colleagues [14].

3.1.2. NSN oocytes

The NSN (GV) antral spectrum (Fig. 3B) in the protein absorption region was mainly characterized by the same components found in the SN type spectrum. Only minor spectral differences were detected during NSN oocytes maturation up to MII formation, involving the components around 1625 cm^{-1} and at 1690 cm^{-1} (β-sheet structures and/or protein–protein interactions) that showed a lower intensity than those observed for the SN oocytes. As discussed above, the component at 1625 cm^{-1} could reflect the formation of the meiotic spindle. Interestingly, no appreciable differences between MI and MII were detected for the NSN oocytes, suggesting a reduced new protein synthesis in this span of time. This result could reflect impairments in the processes of meiotic spindle formation and functioning, crucial to the further embryo development subsequent to fertilization.

Concerning the lipid response, in the case of NSN oocytes the CH_2 and CH_3 bands were seen to vary in intensity during the oocyte maturation (data not shown). In particular, the CH_2 spectral components (2922 and 2852 cm^{-1}) were found to increase in intensity up to NSN oocyte MII, suggesting the presence—at this stage—of a high content of long chain saturated fatty acids, in agreement with what reported for oocytes by Wood and colleagues [14]. Moreover, differences in the spectral features of the band between 3020 and 3000 cm^{-1}, due to the CH stretching of unsaturated acyl chains [14,34], were observed during NSN oocytes maturation. In particular, the antral and MI-derived NSN oocytes were characterized by a single peak around 3013 cm^{-1}, while MII oocytes showed two peaks respectively at 3016 cm^{-1} and at 3010 cm^{-1}. These results might suggest changes in the composition of unsaturated fatty acids, reflecting in particular the number of double bonds in the fatty acid chain [46]. We should note that these lipids increase membrane fluidity, enabling rapid oocyte division after fertilization [14 and references therein].

3.1.3. Multivariate analysis in the SN and NSN protein and lipid spectral regions

The spectroscopic results have been validated by the PCA–LDA approach, performed on the measured spectra between 1800 and 1500 cm^{-1}, where the Amide I and Amide II protein bands occur. In the case of SN oocytes, a spectral segregation into separated clusters was obtained with accuracy of 93.5% (Fig. 4A). The wavenumbers displaying the highest PCA–LDA weight occurred at 1658 cm^{-1} (α-helix; weight 0.99) and at 1622 cm^{-1} (β-sheet structures and/or protein–protein interactions; weight 0.86), as shown in Table 1. Concerning the NSN oocytes, an excellent segregation with accuracy of 100% (Fig. 4B) was found, with the most relevant wavenumbers occurring at 1652 cm^{-1} (α-helix; weight 0.94), 1635 cm^{-1} (intramolecular β-sheet; weight 0.73) and at 1628 cm^{-1} (β-sheet structures and/or protein–protein interactions; weight 0.70). It should be noted that in the NSN oocytes the component due to β-sheet structures and/or protein–protein interactions has been found to have a discrimination weight lower than that observed for SN oocytes (see Table 1), in agreement with the direct inspection of the spectral data.

Moreover, we compared by PCA–LDA the spectra of the two types of oocytes isolated at the same maturation stage, as illustrated in Fig. 4C. This analysis indicated that the highest separation between SN and NSN oocytes is found at MI, with a classification accuracy of 92%. Noteworthy, in the 1800–1500 cm^{-1} spectral range the discriminating wavenumber with the highest weight (1.0) has been found at 1739 cm^{-1}, corresponding to the ester carbonyl absorption, whose content is different in MI derived SN and NSN oocytes.

To better investigate the lipid response during SN and NSN maturation, we performed also the PCA–LDA analysis in the spectral range between 3050 and 2800 cm^{-1}.

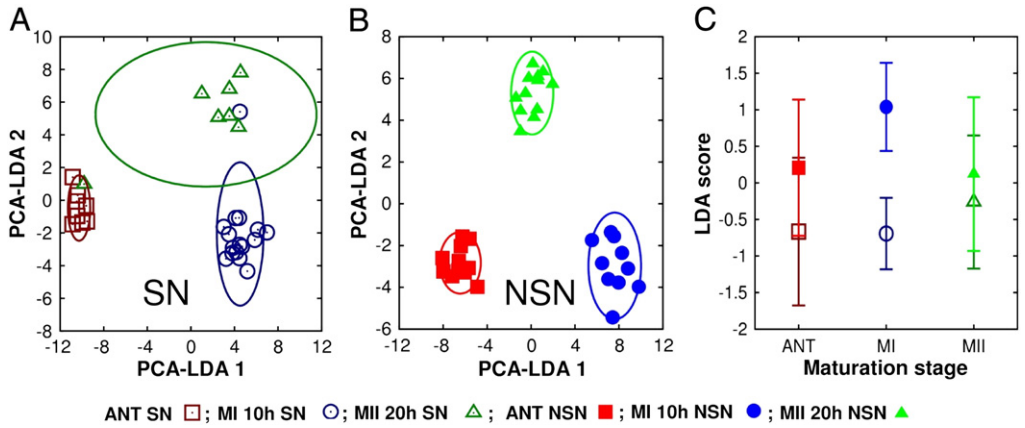

Fig. 4. PCA–LDA analysis of SN and NSN oocytes in the protein absorption region. The PCA–LDA analysis has been performed on measured FTIR absorption spectra in the region between 1800 and 1500 cm^{-1}. Clustering 2D plots of SN (A) and NSN (B) oocytes taken at different maturation stages. The semi-axes of the ellipses in 2D plots correspond to two standard deviations of the data. In (C), SN and NSN separation, given as LDA scores with their standard deviations, is reported at each maturation stage.

In the case of SN oocytes (Fig. 5A) a discrimination accuracy of 77% was found, with the wavenumber carrying the highest weight (1.0) at 2938 cm^{-1}, that might reflect variations in the oocyte cholesterol and/or phospholipid content [44,45], as discussed above.

Interestingly, the analysis of the NSN oocytes (Fig. 5B) led to a higher classification accuracy, namely 85%, with the highest weights at 2920 cm^{-1} (weight 1.0), due to the antisymmetric CH_2 stretching, at 3018 cm^{-1} (weight 0.95), assigned to CH stretching of unsaturated fatty acids [14,34,46], and at 2937 cm^{-1} (weight 0.73), again assigned to cholesterol and / or phospholipids [44,45].

It was, then, interesting to compare the lipid response for the two types of oocytes at each maturation stage (see Fig. 5C). For all stages the discrimination accuracy was higher than 80%. In particular, at the antral GV and MII stages, the wavenumbers carrying the highest weight (higher than 0.7) were the components around 2932 and 2936 cm^{-1}, likely due to phospholipids and cholesterol [44,45,47], while at MI the highest weight (1.0) was found for the CH stretching of unsaturated fatty acids, around 3015 cm^{-1} [46]. These results, all together, clearly indicate that significant differences in the lipid composition characterized the two types of oocytes at each stage of maturation.

3.2. Nucleic acid variations during NSN and SN oocyte maturation

To investigate the response of nucleic acids during oocyte maturation, we analyzed the FTIR absorption in the spectral region between 1000 and 800 cm^{-1}, which is mainly characterized by the absorptions of RNA and DNA vibrational modes [36]. We focalized, in particular, on this spectral range since it is less crowded than that between 1400 and 1000 cm^{-1}, where the spectra are very complex due to the absorption not only of nucleic acids, but also of several other biomolecules, as phospholipids and carbohydrates, making it difficult the band assignment. For this reason, we only reported the results of the statistical

Table 1
Marker bands of SN and NSN oocyte maturation process. Peak positions of the marker bands of SN and NSN oocyte maturation, taken from second derivative spectra and PCA–LDA analysis. PCA–LDA weights are also reported.

SN			NSN			Assignment
Peak position from second derivative spectra (cm^{-1})	Wavenumbers from PCA–LDA (absorption spectra)		Peak position from second derivative spectra (cm^{-1})	Wavenumbers from PCA–LDA (absorption spectra)		
	cm^{-1}	Weight		cm^{-1}	Weight	
3015	3015[a]	1.00	3016	3015[a]	1.00	CH stretching (unsaturated fatty acids)
				3018	0.95	
2937	2936[a]	0.79 (GV)	2937	2936[a]	0.79 (GV)	CH_2 antisymmetric stretching (cholesterol)
	2936[a]	1.00 (MII) 1.00		2936[a]	1.00 (MII)	and CH_3 Fermi resonance (phospholipids)
	2938			2937	0.73	
-	2932[a]	1.00 (GV)	2931	2932[a]	1.00 (GV)	CH_3 Fermi resonance and CH_2 antisymmetric stretching (phospholipids)
			2922	2920	1.00	CH_2 antisymmetric stretching (acyl chains)
1742	1739[a]	1.00	1742	1739[a]	1.00	CO stretching (esters)
1658	1658	0.99	1658	1652	0.94	CO stretching (protein α-helices)
	1656	0.71				
1639	1641	0.73	1639	1635	0.73	CO stretching (protein β-sheets)
~ 1625	1622	0.86	~ 1625	1628	0.70	CO stretching (protein β-sheets; protein–protein interactions)
922	926[a]	1.00	921	926[a]	1.00	Ribose ring
			898, 895	894	0.77	Deoxyribose ring
886	886	0.75	884	880	1.00	CH_2 rocking (polyadenylic acid)
860	859	0.83				CH_2 rocking (polyadenylic acid)
	861	0.71				
854	855[a]	0.97	854	855[a]	0.97	NH out of plane (adenine)
820	821[a]	0.87	818, 824	821[a]	0.87	N-type/S-type sugar marker; polyadenylic acid
	817	1.00				

[a] Wavenumbers from the PCA–LDA analysis resulting from the comparison between SN and NSN oocytes (see text). GV = germinal vesicle (antral) derived oocytes; MII = Metaphase II derived oocytes.

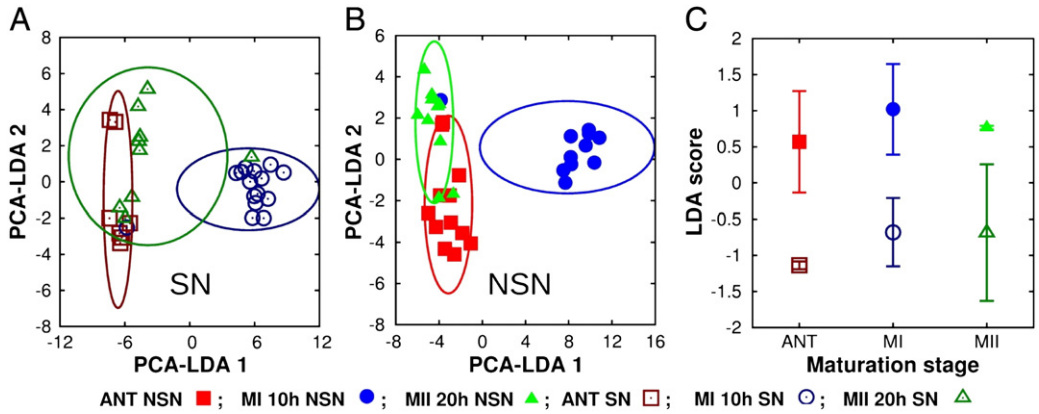

Fig. 5. PCA–LDA analysis of SN and NSN oocytes in the lipid absorption region. The PCA–LDA analysis has been performed on measured FTIR absorption spectra in the region between 3050 and 2800 cm^{-1}. Clustering 2D plots of SN (A) and NSN (B) oocytes taken at different maturation stages. The semi-axes of the ellipses in 2D plots correspond to two standard deviations of the data. In (C), SN and NSN separation, given as LDA scores with their standard deviations, is reported at each maturation stage.

analysis of the data between 1400 and 1000 cm^{-1}, to confirm the findings obtained in the low frequency range for nucleic acids.

In Fig. 6 the second derivative spectra of the NSN and SN oocytes—between 1000 and 800 cm^{-1}—are reported at different maturation stages.

3.2.1. NSN oocytes

The spectrum of the NSN (GV) type oocytes (Fig. 6A) taken at the antral stage displays a triplet at 975 cm^{-1}, 966 cm^{-1} and 951 cm^{-1}, due to the CC stretching vibration of the DNA backbone mainly in the A-form [13,36,48]. Moreover, the bands at 921 cm^{-1} (ribose ring) and at 895 cm^{-1} (deoxyribose ring), simultaneously present in the spectrum, are indicative of the occurrence of a DNA/RNA hybrid, which is known to assume an A-DNA conformation [13,36,48]. These results suggest that, at the antral stage, the NSN oocytes are transcriptionally active, as expected [49]. In addition, at lower frequencies, three important bands fall respectively at 884 cm^{-1}, due to the CH_2 rocking vibration of polyadenylic acid, at 870 cm^{-1}, due to the NH out of plane vibration of adenine, and at 850 cm^{-1} that can be assigned to CH out of plane vibration of uracil and to the NH out of plane vibration of adenine [50]. Moreover, a weak component around 860 cm^{-1} is observed and can be assigned to CH_2 rocking vibration of polyadenylic acid [50]. The relative intensities of these components could provide information on the mRNA polyadenylation extent, an important mechanism that regulates transcription. In particular, the cytoplasmic extension of maternal mRNA polyA tails, stored during oocyte growth and maturation, controls the translational activation of these "dormant" mRNAs after fertilization. Interestingly, polyadenylation requires, in addition to the highly conserved AAUAAA hexanucleotide, also a more variable uracil rich element—the so-called cytoplasmic polyadenylation element (CPE) [51]. We can, therefore, suggest that the 850 cm^{-1} band—due to both uracil and adenine—could be taken as marker band of polyadenylation.

Furthermore, in the NSN (GV) spectrum two peaks are observed at 836 cm^{-1} and at 824 cm^{-1} that can be assigned to two DNA S-type sugar puckering modes, sensitive to changes in the DNA sugar conformation induced by cytosine methylation, as reported by Banyay and Graslund [52]. These authors found that fully demethylated DNA decamers, taken as a model of CpG islands, displayed a single marker band, around 830 cm^{-1}, of S-type sugars, while a splitting of this band into two components was observed as a consequence of cytosine methylation. These components change in peak position and intensity depending on the methylation degree and reflect the coexistence of two main puckers within the S-type sugars in the methylated DNA [52]. Therefore, the peaks occurring at 836 cm^{-1} and 824 cm^{-1} in NSN oocytes could reflect a partially methylated DNA at the antral stage.

Interestingly, the above spectral signatures were found to change during oocyte maturation, as described in the following.

In NSN-derived MI oocytes, the components assigned to the CC stretching of DNA backbone consisted in a weak shoulder at 977 cm^{-1}, a

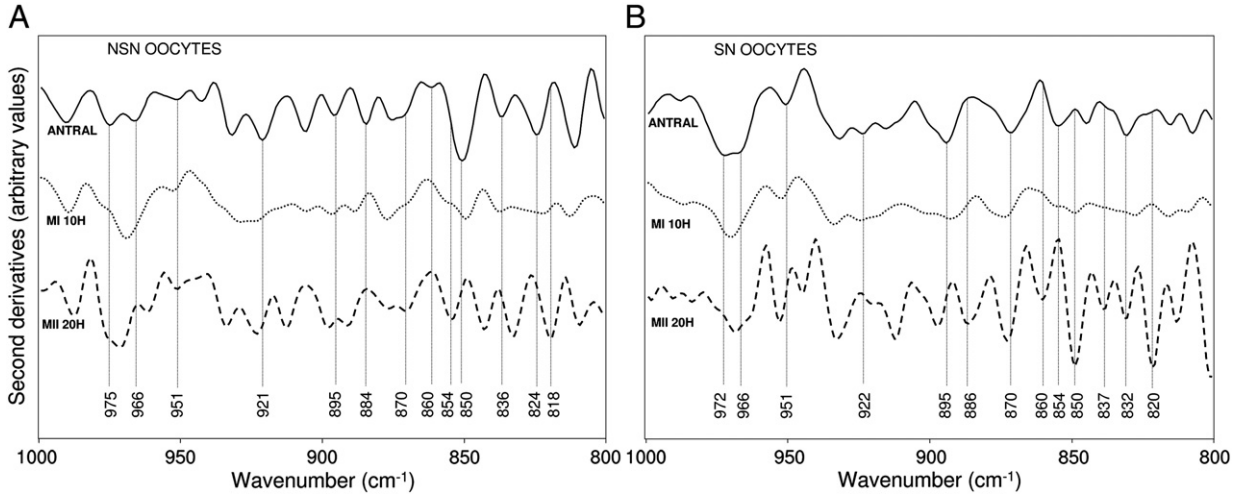

Fig. 6. Second derivative absorption spectra of NSN and SN oocytes in the nucleic acid absorption region. The second derivatives of the FTIR absorption spectra of NSN (A) and SN (B) single oocytes measured at the antral (continuous line), MI (dotted line) and MII (dashed line) stages are shown, between 1000 and 800 cm^{-1}. The most significant spectral components, whose assignment is reported in Table 1, are indicated. For comparison, spectra have been normalized at the tyrosine peak around 1516 cm^{-1}.

new well resolved component at 969 cm^{-1}, due to B-DNA, and by the peak at 951 cm^{-1}. In particular, the upshift of the 966 cm^{-1} triplet component to 969 cm^{-1} might suggest a simultaneous increase of B-DNA and a decrease of A-DNA, indicating a conformational DNA transition at this stage. Interestingly also the components due to ribose ring (around 921 cm^{-1}) and deoxyribose ring (around 895 cm^{-1}) vibrations displayed an appreciably lower intensity, suggesting that a reduced transcriptional activity occurred in NSN oocytes at this maturation stage. Moreover, the two components at 884 cm^{-1} and 860 cm^{-1} (both due to CH_2 rocking vibration of polyadenylic acid) completely disappeared, while the bands around 870 cm^{-1} (NH out of plane vibration of adenine) and 850 cm^{-1} (CH out of plane vibration of uracil and NH out of plane vibration of adenine) also decreased in intensity. These data seem to suggest that the NSN oocytes at the MI stage enter into a transcriptional "standby" state. Moreover, the two components at 836 cm^{-1} and around 824 cm^{-1} showed a decreased intensity compared with those found at the antral stage, thus suggesting a reduction in the CpG island methylation. Likely, the simultaneous reduction of DNA methylation and transcriptional activity seems to prepare the system for a subsequent activation of those genes that necessarily must be expressed.

At MII stage, NSN oocytes still showed the three components at 975 cm^{-1}, 969 cm^{-1} and at 951 cm^{-1}, due to the CC stretching vibrations of the DNA backbone, already observed at MI, again indicating the coexistence of DNA in A and in B form. It is noteworthy to remark also the increased intensity of the bands around 921 cm^{-1} (ribose ring) and at 898 cm^{-1} (deoxyribose ring), that suggests an increased transcriptional activity of NSN oocytes at this stage.

Significant spectral changes were also observed for the bands involved in polyadenylation. In particular, the band at 884 cm^{-1} (CH_2 rocking vibration of polyadenylic acid) was still absent at MII, while the band at 870 cm^{-1} (NH out of plane vibrations of adenine) [50] increased in intensity. Moreover, the component at 850 cm^{-1} (NH out of plane vibration of adenine; CH out of plane vibration of uracil) [50] disappeared, while a new band appeared at 854 cm^{-1} (NH out of plane vibration of adenine possibly not involved in polyA tail formation) [53]. Taken together, these results could indicate a reduced extent of polyadenylation starting from MI oocytes. Noteworthy, these last data suggest that the failure of NSN oocytes to resume meiosis can be ascribed to an inadequate level of polyadenylation.

Concerning CpG island methylation, a single strong band at 832 cm^{-1} (instead of two splitted components) might reflect a negligible methylation level for the NSN-derived MII.

The information obtained from the FTIR analysis suggests, therefore, that the NSN oocyte maturation is characterized by a higher transcriptional activity at MII than at the antral stage—as pointed out by a negligible DNA methylation at this stage—and by a lower level of polyadenylation of mRNAs, whose main marker band at 884 cm^{-1} is absent at MII.

3.2.2. SN oocytes

The spectrum of the antral SN (GV) oocytes (Fig. 6B) is characterized by the triplet (972 cm^{-1}, 966 cm^{-1}, 951 cm^{-1}) assigned to the CC stretching vibration of the DNA backbone mainly in the A form [36], even though the 972 cm^{-1} and 966 cm^{-1} components are less resolved than in the antral NSN oocyte spectrum. In addition, the low intensity band around 922 cm^{-1} (ribose ring) and the broad component at 895 cm^{-1} with a shoulder around 899 cm^{-1} (deoxyribose ring) [36] could be indicative of a low level of DNA/RNA hybrid formation [13,48]. These results taken together suggest a reduced extent of transcriptional activity of the SN versus the NSN oocytes, in agreement with what is reported in the literature [54,55].

Interestingly, no evidence of mRNA polyadenylation was found in the antral SN oocyte spectra, as indicated from the lack of the ~884 cm^{-1} and 860 cm^{-1} bands, both due to CH_2 rocking vibration of polyadenylic acid [50]. Moreover, the presence of the band at 854 cm^{-1} assigned to NH out of plane vibration of adenine (observed also in the MII derived from NSN oocytes) might suggest the presence of free adenine, not involved in polyadenylation. Accordingly, whenever the pattern of the polyadenylation bands is absent, the absorption due to the uracil involved in the cytoplasmic polyadenylation element (850 cm^{-1}) is absent too. In addition, the single broad band at 832 cm^{-1} with a weak shoulder around 837 cm^{-1} (S type DNA sugar puckering mode) suggests a partial CpG methylation that will increase dramatically at MII.

The spectrum of the MI displays a significant reduction of the A-DNA content and a simultaneous increase of B-DNA, as shown by the absence of the triplet component around 975 cm^{-1} and by the upshift of the band at 966 cm^{-1} to 969 cm^{-1}, marker band of B-DNA. No appreciable evidence of DNA/RNA hybrid is found, as indicated by the negligible ribose component around 922 cm^{-1}, suggesting a "standby" state of transcriptional activity, as observed for NSN at the same maturation stage. In addition, we still observed the adenine 870 cm^{-1} component and the rising of the 850 cm^{-1} band, due to uracil and adenine. Furthermore, the two S-type DNA sugar peaks at about 832 cm^{-1} and 837 cm^{-1} were also present, indicating that a partial CpG methylation was likely occurring.

At MII, the presence of the three components at 975 cm^{-1} (absent at MI stage), 969 cm^{-1} and 953 cm^{-1} (all due to the CC stretching DNA backbone) indicates the coexistence of DNA in A and in B form, as discussed for NSN oocytes. The simultaneous presence of the ribose shoulder around 922 cm^{-1} (negligible at MI) and of the deoxyribose 899 cm^{-1} band points to transcriptional activity at this stage of maturation, even if at a lower level than in the NSN-derived MII oocytes. This is suggested by the presence of the two DNA S-type sugar peaks at 832 cm^{-1} and at 837 cm^{-1}, which are evidence of cytosine methylation.

New bands at 886 cm^{-1} and at 860 cm^{-1} (due to polyadenylic acid absorption), absent in the spectrum of NSN-derived MII, were instead observed in SN-derived MII, together with a strong increase of the adenine and uracil bands around 870 cm^{-1} and 850 cm^{-1}. These results could indicate the well known accumulation of polyA mRNA during oocyte maturation.

Briefly, we would like to suggest that SN oocyte transcriptional activity was maintained at lower levels during the whole maturation process compared to NSN oocytes, being almost absent at MI. During the last stages of oocyte maturation, SN oocytes displayed significant polyA content reflecting the accumulation of maternal mRNAs with polyA tails, a phenomenon that is crucial to support early embryonic development. Noteworthy, NSN-derived MII oocytes did not display the main 886 cm^{-1} and 860 cm^{-1} marker bands of polyadenylation. These last data are highly supportive of the unique prospective capacity of SN oocytes to fully sustain embryo development.

3.2.3. Multivariate analysis in the NSN and SN nucleic acid spectral region

As discussed for the protein response, we performed the combined PCA–LDA analysis in the nucleic acid spectral region, between 1000 and 800 cm^{-1}, of the different oocyte maturation stages.

The NSN oocytes displayed a segregation into three separated clusters, each corresponding to the different maturation stages, with a classification accuracy of about 80% (Fig. 7A). The wavenumbers that carry the highest weights are reported in Table 1. We should remark that the band bringing the highest weight (1.00) is around 880 cm^{-1}, which can be assigned to polyadenylic acid [50]. Interestingly, its intensity varies dramatically during NSN oocyte maturation, being present only at the antral stage and almost disappearing upon maturation up to MII. In addition, a high weight of 0.77 was also found for the 894 cm^{-1} band, due to the deoxyribose ring vibration [50].

Concerning the SN oocytes, the PCA–LDA analysis showed an excellent segregation of the data into well separated clusters for each maturation stage, with an accuracy of about 97% (Fig. 7B). Among the wavenumbers carrying the highest weights (Table 1), the analysis found

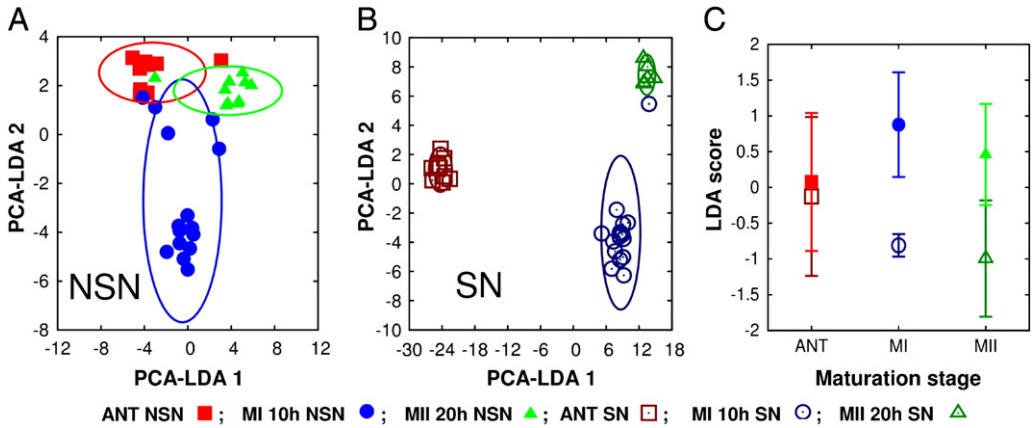

Fig. 7. PCA–LDA analysis of NSN and SN oocytes in the nucleic acid absorption region. The PCA–LDA analysis has been performed on measured FTIR absorption spectra in the region between 1000 and 800 cm^{-1}. Clustering 2D plots of NSN (A) and SN (B) oocytes taken at different maturation stages. The semi-axes of the ellipses in 2D plots correspond to two standard deviations of the data. In (C), NSN and SN separation, given as LDA scores with their standard deviations, is reported at each maturation stage.

peaks around 817 cm^{-1} (weight 1.00) and at 859 cm^{-1} (weight 0.83). While the peak at 859 cm^{-1} is assigned to the CH_2 rocking vibration of polyadenylic acid [50], the assignment of the 817 cm^{-1} band is not unequivocal. Indeed, this band can be due to overlapping contributions of DNA and polyadenylic acid vibrational modes [36,50]. However, these two peaks change dramatically during SN oocyte maturation, as seen by the direct inspection of the spectra (see Fig. 6B).

We also compared by PCA–LDA the infrared response of the two types of oocytes taken at the same maturation stage (see Fig. 7C). Noteworthy, the highest spectral variance involved at each time the polyadenylation bands and the transcription markers. The largest spectral distance between NSN and SN oocytes was found at MI (classification accuracy 92%), mainly due to the marker bands of A-DNA during transcription. Indeed, from this "standby" state the two types of oocytes will move toward two separate pathways: the SN oocytes, with their storage of maternal mRNAs with polyA tails, ready for the subsequent activation and development, and the NSN oocytes kept in a unsuccessful transcriptional state that does not lead to new protein synthesis, nor to properly adenylated mRNA storage. This situation might be prospective of the two-blastomere developmental block. To support this important result, we reported in Fig. 8 the analysis of the infrared response of NSN and SN oocytes at each time of maturation, all together. In particular, the analysis in the nucleic acid absorption region enabled us to obtain a good discrimination (accuracy of 89%) with a clear-cut separation into two main groups: one containing just only the SN oocytes collected at MII stage (likely those having a full developmental capacity) and a second group with all the other SN and NSN stages. The wavenumbers carrying the highest weight were found at 926 cm^{-1} due to ribose vibration (weight 1.00) and at 855 cm^{-1} due to adenine vibration (weight 0.97), both reflecting again transcription and polyadenylation processes.

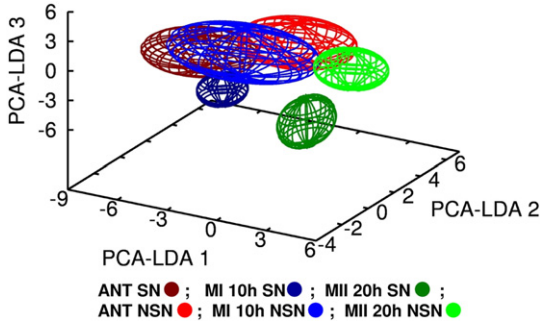

Fig. 8. PCA–LDA analysis of SN and NSN oocytes in the nucleic acid absorption regions. The PCA–LDA analysis has been carried out on measured FTIR absorption spectra. Clustering of SN and NSN oocytes at each maturation stage obtained for the nucleic acid absorption region, between 1000 and 800 cm^{-1}. The semi-axes of ellipsoids in the 3D score plots correspond to two standard deviations of the data along each direction.

Interestingly, these results were further confirmed by the PCA–LDA analysis performed on the 1400–1000 cm^{-1} spectral region. In particular in the case of NSN oocytes, the wavenumber carrying the highest discrimination weight (1.0) resulted that at 1305 cm^{-1}, assigned to free adenine (possibly not involved in polyadenylation) [50], whose intensity was higher at MII, in agreement with the adenine vibrational mode at 870 cm^{-1}, discussed above. These findings likely confirm that an inadequate polyadenylation level could impair the embryonic development of NSN oocytes.

4. Conclusions

In this work we studied single SN and NSN murine oocytes, taken at three different maturation stages, by FTIR microspectroscopy combined to multivariate PCA–LDA.

The most significant differences were found in the lipid and nucleic acid absorption regions. The analysis of the lipid response suggested that SN and NSN oocytes are characterized by a different lipid composition that might confer to the oocyte a different division ability after fertilization. For this reason, lipids could represent important molecular markers of oocyte developmental capacity [14,43].

Concerning nucleic acid analysis, the spectral components with the highest statistical significance were those reflecting changes in transcriptional activity and polyadenylation extent during maturation. Our findings suggest that NSN oocytes maintained, during all the maturation process, a higher transcriptional activity than the SN type. Otherwise, SN derived MII oocytes showed a significant polyA content that could reflect the storage of maternal mRNAs with polyA tails, crucial for the subsequent early embryonic development.

Moreover, the PCA–LDA analysis enabled us to identify the maturation stage, namely MI, where an evident separation between the two types of oocytes was found, strongly suggesting that the maturation of the antral SN and NSN oocytes up to MI stage can be considered a crucial "checkpoint" when some molecular components and/or processes possibly rearrange to determine oocyte fate and destiny toward, or not, meiotic resumption. Indeed, from this stage the SN oocytes with their maternal mRNAs, appropriately polyadenylated, are ready for the activation and development. The NSN oocytes, instead, lacking a properly polyadenylated maternal mRNAs, are kept in an unsuccessful transcriptional state (see Fig. 8).

Acknowledgments

D. A. and M. M. are indebted to Fondazione IRCCS Policlinico San Matteo, Pavia (I) for the supporting scholarship. D. A. acknowledges a postdoctoral fellowship of the University of Milano-Bicocca. S.M. D. acknowledges the financial support of the FAR (Fondo di Ateneo per la Ricerca) of the University of Milano-Bicocca (I).

Appendix A. Supplemetary data

Supplementary data to this article can be found online at doi:10.1016/j.bbamcr.2011.03.009.

References

[1] B.A. Mattson, D.F. Albertini, Oogenesis: chromatin and microtubule dynamics during meiotic prophase, Mol. Reprod. Dev. 25 (1990) 374–383.
[2] P. Debey, M.S. Szollosi, D. Szollosi, D. Vautier, A. Girousse, D. Besombes, Competent mouse oocytes isolated from antral follicles exhibit different chromatin organization and follow different maturation dynamics, Mol. Reprod. Dev. 36 (1993) 59–74.
[3] A.M. Mandl, Preovulatory changes in the oocyte of the adult rat, Proc. R. Soc. Lond. 158 (1962) 105–118.
[4] N. Crozet, J. Motlik, D. Szollosi, Nucleolar fine structure and RNA synthesis in porcine oocytes during early stages of antrum formation, Biol. Cell 41 (1981) 35–42.
[5] B. Lefevre, A. Gougeon, F. Nome, J. Testart, In vivo changes in oocyte germinal vesicle related to follicular quality and size at mid-follicular phase during stimulated cycles in the cynomolgus monkey, Reprod. Nutr. Dev. 29 (1989) 523–531.
[6] V. Parfenov, G. Potchukalina, L. Dudina, D. Kostyuchek, M. Gruzova, Human antral follicles: oocyte nucleus and the karyosphere formation (electron microscopic and autoradiographic data), Gamete Res. 22 (1989) 219–231.
[7] M. Zuccotti, A. Piccinelli, P. Giorgi Rossi, S. Garagna, C.A. Redi, Chromatin organization during mouse oocyte growth, Mol. Reprod. Dev. 41 (1995) 479–485.
[8] M. Zuccotti, S. Garagna, V. Merico, M. Monti, C.A. Redi, Chromatin organisation and nuclear architecture in growing mouse oocytes, Mol. Cell. Endocrinol. 234 (2005) 11–17.
[9] T. Nakamura, J.G. Kelly, J. Trevisan, L.J. Cooper, A.J. Bentley, P.L. Carmichael, A.D. Scott, M. Cotte, J. Susini, P.L. Martin-Hirsch, S. Kinoshita, N.J. Fullwood, F.L. Martin, Microspectroscopy of spectral biomarkers associated with human corneal stem cells, Mol. Vis. 16 (2010) 359–368.
[10] M. Monti, C.A. Redi, Oogenesis specific genes (Nobox, Oct4, Bmp15, Gdf9, Oogenesin1 and Oogenesin2) are differently expressed during natural and gonadotropin-induced mouse follicular development, Mol. Reprod. Dev. 76 (2009) 994–1003.
[11] M. Monti, S. Garagna, C.A. Redi, M. Zuccotti, Gonadotropins affect Oct4 gene expression during mouse oocyte growth, Mol. Reprod. Dev. 73 (2006) 685–691.
[12] D. Ami, A. Natalello, G. Taylor, G. Tonon, S.M. Doglia, Structural analysis of protein inclusion bodies by Fourier transform infrared microspectroscopy, Biochim. Biophys. Acta 1764 (2006) 793–799.
[13] D. Ami, T. Neri, A. Natalello, P. Mereghetti, S.M. Doglia, M. Zanoni, M. Zuccotti, S. Garagna, C.A. Redi, Embryonic stem cell differentiation studied by FTIR spectroscopy, Biochim. Biophys. Acta 1783 (2008) 98–106.
[14] B.R. Wood, T. Chernenko, C. Matthäus, M. Diem, C. Chong, U. Bernhard, C. Jene, A.A. Brandli, D. McNaughton, M.J. Tobin, A. Trounson, O. Lacham-Kaplan, Shedding new light on the molecular architecture of oocytes using a combination of synchrotron Fourier transform-infrared and Raman spectroscopic mapping, Anal. Chem. 80 (2008) 9065–9072.
[15] K. Thumanu, W. Tanthanuch, C. Lorthongpanich, P. Heraud, R. Parnpai, FTIR microspectroscopic imaging as a new tool to distinguish chemical composition of mouse blastocyst, J. Mol. Struct. 933 (2009) 104–111.
[16] M.J. Walsh, A. Hammiche, T.G. Fellous, J.M. Nicholson, M. Cotte, J. Susini, N.J. Fullwood, P.L. Martin-Hirsch, M.R. Alison, F.L. Martin, Tracking the cell hierarchy in the human intestine using biochemical signatures derived by mid-infrared microspectroscopy, Stem Cell Res. 3 (2009) 15–27.
[17] L.P. Choo, D.L. Wetzel, W.C. Halliday, M. Jackson, S.M. LeVine, H.H. Mantsch, In situ characterization of beta-amyloid in Alzheimer's diseased tissue by synchrotron Fourier transform infrared microspectroscopy, Biophys. J. 71 (1996) 1672–1679.
[18] J. Kneipp, L.M. Miller, M. Joncic, M. Kittel, P. Lasch, M. Beekes, D. Naumann, In situ identification of protein structural changes in prion-infected tissue, Biochim. Biophys. Acta 1639 (2003) 152–158.
[19] D. Ami, A. Natalello, A. Zullini, S.M. Doglia, Fourier transform infrared microspectroscopy as a new tool for nematode studies, FEBS Lett. 576 (2004) 297–300.
[20] D. Ami, L. Bonecchi, S. Calì, G. Orsini, G. Tonon, S.M. Doglia, FTIR study of heterologous protein expression in recombinant *Escherichia coli* strains, Biochim. Biophys. Acta 1624 (2003) 6–10.
[21] L. Diomede, G. Cassata, F. Fiordaliso, M. Salio, D. Ami, A. Natalello, S.M. Doglia, A. De Luigi, M. Salmona, Tetracycline and its analogues protect *Caenorhabditis elegans* from β amyloid-induced toxicity by targeting oligomers, Neurobiol. Dis. 40 (2010) 424–431.
[22] W. Tanthanuch, K. Thumanu, C. Lorthongpanich, R. Parnpai, P. Heraud, Neural differentiation of mouse embryonic stem cells studied by FTIR spectroscopy, J. Mol. Struct. 967 (2010) 189–195.
[23] M.J. German, H.M. Pollock, B. Zhao, M.J. Tobin, A. Hammiche, A. Bentley, L.J. Cooper, F.L. Martin, N.J. Fullwood, Characterization of putative stem cell populations in the cornea using synchrotron infrared microspectroscopy, Invest. Ophthalmol. Vis. Sci. 47 (2006) 2417–2421.
[24] A.J. Bentley, T. Nakamura, A. Hammiche, H.M. Pollock, F.L. Martin, S. Kinoshita, N.J. Fullwood, Characterization of human corneal stem cells by synchrotron infrared micro-spectroscopy, Mol. Vis. 13 (2007) 237–242.
[25] M.J. Walsh, T.G. Fellous, A. Hammiche, W.R. Lin, N.J. Fullwood, O. Grude, F. Bahrami, J.M. Nicholson, M. Cotte, J. Susini, H.M. Pollock, M. Brittan, P.L. Martin-Hirsch, M.R. Alison, F.L. Martin, Fourier transform infrared micro-spectroscopy identifies symmetric PO(2)(-) modifications as a marker of the putative stem cell region of human intestinal crypts, Stem Cells 26 (2008) 108–118.
[26] J.K. Pijanka, D. Kumar, T. Dale, I. Yousef, G. Parkes, V. Untereiner, Y. Yang, P. Dumas, D. Collins, M. Manfait, G.D. Sockalingum, N.R. Forsyth, J. Sulé-Suso, Vibrational spectroscopy differentiates between multipotent and pluripotent stem cells, Analyst 135 (2010) 3126–3132.
[27] E. Voronina, G.M. Wessel, The regulation of oocytes maturation, Curr. Top. Dev. Biol. 58 (2003) 53–110.
[28] T. Fearn, Discriminant analysis, in: J.M. Chalmers, P.R. Griffiths (Eds.), Handbook of Vibrational Spectroscopy, Wiley, New York, 2002, pp. 2086–2093.
[29] M.J. Walsh, M.N. Singh, H.M. Pollock, L.J. Cooper, M.J. German, H.F. Stringfellow, N. J. Fullwood, E. Paraskevaidis, P.L. Martin-Hirsch, F.L. Martin, ATR microspectroscopy with multivariate analysis segregates grades of exfoliative cervical cytology, Biochem. Biophys. Res. Commun. 352 (2007) 213–219.
[30] E. Christians, M. Boiani, S. Garagna, C. Dessy, C.A. Redi, J.P. Renard, M. Zuccotti, Gene expression and chromatin organization during mouse oocyte growth, Dev. Biol. 207 (1999) 76–85.
[31] A.C. Rencher, Methods of Multivariate Analysis, Wiley, Hoboken, 2002.
[32] F.L. Martin, M.J. German, E. Wit, T. Fearn, N. Ragavan, H.M. Pollock, Identifying variables responsible for clustering in discriminant analysis of data from infrared microspectroscopy of a biological sample, J. Comput. Biol. 14 (2007) 1176–1184.
[33] L. Eriksson, E. Johansson, N. Kettaneh-Wold, J. Trygg, C. Wikstrom, S. Wold, Multivariate and Megavariate Data Analysis Basic Principles and Applications, Umetrics Academy, San Jose, 2006.
[34] H.L. Casal, H.H. Mantsch, Polymorphic phase behaviour of phospholipid membranes studied by infrared spectroscopy, Biochim. Biophys. Acta 779 (1984) 381–401.
[35] J.L.R. Arrondo, F.M. Goni, Structure and dynamics of membrane proteins as studied by infrared spectroscopy, Prog. Biophys. Mol. Biol. 72 (1999) 367–405.
[36] M. Banyay, M. Sarkar, A. Graslund, A library of IR bands of nucleic acids in solution, Biophys. Chem. 104 (2003) 477–488.
[37] P.I. Haris, F. Severcan, FTIR spectroscopic characterization of protein structure in aqueous and non-aqueous media, J. Mol. Catal., B Enzym. 7 (1999) 207–221.
[38] A. Barth, C. Zscherp, What vibrations tell us about proteins, Q. Rev. Biophys. 35 (2002) 369–430.
[39] H. Picton, D. Briggs, R. Gosden, The molecular basis of oocyte growth and development, Mol. Cell. Endocrinol. 145 (1998) 27–37.
[40] H. Pan, M.J. O'Brien, K. Wigglesworth, J.J. Eppig, R.M. Schultz, Transcript profiling during mouse oocyte development and the effect of gonadotropin priming and development in vitro, Dev. Biol. 286 (2005) 493–506.
[41] M. Ma, X. Guo, F. Wang, C. Zhao, Z. Liu, Z. Shi, Y. Wang, P. Zhang, K. Zhang, N. Wang, M. Lin, Z. Zhou, J. Liu, Q. Li, L. Wang, R. Huo, J. Sha, Q. Zhou, Protein expression profile of the mouse metaphase-II oocytes, J. Proteome Res. 7 (2008) 4821–4830.
[42] Q.Y. Sun, H. Schatten, Regulation of dynamic events by microfilaments during oocyte maturation and fertilization, Reproduction 131 (2006) 193–205.
[43] L. Gentile, M. Monti, V. Sebastiano, V. Merico, R. Nicolai, M. Calvani, S. Garagna, C.A. Redi, M. Zuccotti, Single cell quantitative RT-PCR analysis of Cpt1 and Ctp2 gene expression in mouse antral oocytes and preimplantation embryos, Cytogenet. Genome Res. 105 (2004) 215–221.
[44] R. Marty, C.N. N'soukpoé-Kossi, D.M. Charbonneau, L. Kreplak, H.-A. Tajmir-Riahi, Structural characterization of cationic lipid–tRNA complexes, Nucl. Acids Res. 37 (2009) 5197–5207.
[45] J. Liu, J.C. Conboy, Structure of a gel phase lipid bilayer prepared by the Langmuir–Blodgett/Langmuir–Schaefer method characterized by sum-frequency vibrational spectroscopy, Langmuir 21 (2005) 9091–9097.
[46] E.M. Calvey, R.E. McDonald, S.W. Page, M.M. Mossoba, L.T. Taylor, Evaluation of SFC/FTIR for examination of hydrogenated soybean oil, J. Agric. Food Chem. 39 (1991) 542–548.
[47] M.R. Watry, G.L. Richmond, Effects of halothane on phosphatidylcholine, -ethanolamine, -glycerol, and -serine monolayer order at a liquid/liquid interface, Langmuir 18 (2002) 8881–8887.
[48] D. Ami, A. Natalello, P. Mereghetti, T. Neri, M. Zanoni, M. Monti, S.M. Doglia, C.A. Redi, FT-IR spectroscopy supported by PCA–LDA analysis for the study of embryonic stem cell differentiation, Spectr.-Int. J. 24 (2010) 89–97.
[49] S. Kageyama, H. Liu, N. Kaneko, M. Ooga, M. Nagata, F. Aoki, Alterations in epigenetic modifications during oocyte growth in mice, Reproduction 133 (2007) 85–94.
[50] G.P. Zhizhina, E.F. Oleinik, Infrared spectroscopy of nucleic acids, Russ. Chem. Rev. 41 (1972) 258–280.

[51] E. Seli, M.D. Lalioti, S.M. Flaherty, D. Sakkas, N. Terzi, J.A. Steitz, An embryonic poly (A)-binding protein (ePAB) is expressed in mouse oocytes and early preimplantation embryos, Proc. Natl. Acad. Sci. U.S.A. 102 (2005) 367–372.
[52] M. Banyay, A. Graslund, Structural effects of cytosine methylation on DNA sugar pucker studied by FTIR, J. Mol. Biol. 324 (2002) 667–676.
[53] G.N. Ten, V.I. Baranov, Manifestation of intramolecular proton transfer in imidazole in the electronic vibrational spectrum, J. Appl. Spectr. 75 (2008) 168–173.
[54] R. De La Fuente, M.M. Viveiros, K.H. Burns, E.Y. Adashi, M.M. Matzuk, J.J. Eppig, Major chromatin remodeling in the germinal vesicle (GV) of mammalian oocytes is dispensable for global transcriptional silencing but required for centromeric heterochromatin function, Dev. Biol. 275 (2004) 447–458.
[55] H. Fulka, Z. Novakova, T. Mosko, J. Fulka Jr., The inability of fully grown germinal vesicle stage oocyte cytoplasm to transcriptionally silence transferred transcribing nuclei, Histochem. Cell Biol. 132 (2009) 457–468.